Quantum critical scaling for finite-temperature Mott-like metal-insulator crossover in few-layered MoS₂

Byoung Hee Moon [1,2,*,†] Gang Hee Han,[1,*] Miloš M. Radonjić,[3] Hyunjin Ji,[4] and Vladimir Dobrosavljević[5,‡]

[1]*Department of Physics, Incheon National University, Incheon 22012, Republic of Korea*
[2]*Center for Integrated Nanostructure Physics, Institute for Basic Science (IBS), Suwon 16419, Republic of Korea*
[3]*Institute of Physics Belgrade, University of Belgrade, Pregrevica 118, 11080 Belgrade, Serbia*
[4]*School of Electrical Engineering, University of Ulsan, Ulsan 44610, Republic of Korea*
[5]*Department of Physics and National High Magnetic Field Laboratory, Florida State University, Tallahassee, Florida 32306, USA*

The dominant role of strong electron-electron interactions in driving two-dimensional metal-insulator transitions has long been debated, but its clear experimental demonstration is still not available. Here, we examine the finite-temperature transport behavior of few-layered MoS₂ material in the vicinity of the density-driven metal-insulator transition, revealing previously overlooked universal features characteristic of strongly correlated electron systems. Our scaling analysis, based on the Wigner-Mott theoretical viewpoint, conclusively demonstrates that the transition is driven by strong electron-electron interactions and not disorder, in striking resemblance to what is seen in other Mott systems. Our results provide compelling evidence that transition-metal dichalcogenides provide an ideal testing ground, and should open an exciting avenue for the study of strong correlation physics.

I. INTRODUCTION

Since early experimental demonstrations [1–5] of a metal-insulator transition in two-dimensional systems (2DMITs) in silicon, the pivotal role of electron-electron interactions has been recognized [5] as a key factor. By demonstrating that the salient features of this transition are most pronounced in the cleanest samples, more recent experimental studies [6] provided further evidence that this phenomenon is dominated by this strong electronic correlation, and not disorder, in contrast to early theoretical ideas [7,8]. Despite these advances, several basic issues continued to cause controversy, and the progress remained slow. Most importantly, it is still not completely clear if the basic physical mechanism driving this transition bears much in common with other examples of correlated quantum matter, or whether it is simply an exotic phenomenon specific to two-dimensional electron gases (2DEGs) in semiconductors. To place 2DMITs in the proper perspective, and to more deeply understand the processes underpinning its striking phenomenology, it is of absolute importance to seek other materials and systems displaying similar behavior. To do this, one needs to establish precisely which aspects of 2DMITs represent the universal features of correlation-driven metal-insulator transitions and which ones are specific to a given material-dependent realization.

A physical picture suggesting how strong electronic correlations could drive such a transition is based on the mechanism for Wigner crystallization, leading to the so-called Wigner-Mott scenario for 2DMITs [9–14]. According to this view, in high mobility samples of 2D diluted electron gasses disorder does not play a dominant role for electron localization, except to perhaps help stabilize (pin) the Wigner crystal which is expected to be formed at the lowest densities. The Wigner crystal can be regarded as Mott insulator where carriers form spin 1/2 bound states in the potential well created by Coulomb repulsion of surrounding carriers, so called Wigner-Mott insulator. At higher densities the increased kinetic energy of carriers is eventually able to overcome the Coulomb repulsion, and the Wigner-Mott insulator gives way to the formation of a strongly correlated electron liquid. This perspective, while appealing, has remained controversial, because a controlled microscopic theory is not yet available for the (continuum) 2DEGs, in contrast to more conventional lattice models, where more reliable theoretical results have already started to emerge in the last ten years.

Some further progress in this general direction was achieved by recent studies on 2D molecular organic materials at half-filling (so-called Mott organics) [15], where systematic studies of the correlation-driven metal-insulator transitions were performed, providing intriguing information. These systems are Mott insulators under ambient conditions, but display a transition to a metallic state under moderate pressures, allowing precise and systematic studies of the Mott transition. Most importantly, they are well described by the simplest model of electronic correlation, the single band Hubbard model, making possible direct and very successful comparison with a theory. Here transport experiments revealed several remarkable features, including the scaling of resistivity curves around the so-called quantum Widom line, as well as the

---

*These authors contributed equally to this work.
†Corresponding author: bhmoon@inu.ac.kr
‡Corresponding author: vlad@magnet.fsu.edu

characteristic evolution of the resistivity maxima, confirming in spectacular detail the predictions of recent theoretical studies [16]. Some similarity of this phenomenology with that of 2DMIT in other 2DEG systems has been noted [14], but the precise connection remained controversial and incomplete.

A remarkable opportunity to shed light on the fundamental mechanism for 2DMITs was achieved by the recent discovery of a class of two-dimensional materials based on transition-metal elements, which already displayed a number of spectacular features [17,18]. These materials allow for unique control over material properties, due to their weak van der Waals bonding between monolayers, allowing easy exfoliation and unprecedented device fabrication. In this paper, we focus on a careful and precise study of transport in a two-dimensional electron gas in a few-layer MoS_2 material, and we analyze the results in light of the Mott-transition scenario guided by theory, as inspired by the recent successes in Mott organics [15,19]. The results, which we present below, display remarkable similarity to other 2DEG systems, but our analysis demonstrates that its universal features are, in fact, identical to those established for 2D Mott organics. This firmly establishes the strong electronic correlations as the dominant driving force for the metal-insulator transition, painting a remarkably elegant yet robust physical picture concerning its fundamental character. In the following, we first briefly review what is known for the already established examples of bandwidth driven Mott transitions, and then present our experimental data and carry out the appropriate analysis guided by Mott transition theory. To be clearer, we note that, as the physical density of electrons in 2DEGs is varied, so is the lattice spacing in the Wigner crystal, hence the unit cell occupation remains constant. The Wigner-Mott transition, therefore, should be similar to a bandwidth driven Mott transition, leading to the comparison of experimental results to theoretical results for a bandwidth driven Mott transition using dynamical mean-field theory (DMFT).

Concerning the phenomenology of the Mott transition, much controversy has existed ever since the early days of high-T_c superconductivity, but more recent experimental and theoretical work established certain robust features, as follows. First, the low-temperature transition has first-order character and displays a phase coexistence region below the critical end point at $T = T_c$. The existence of critical end point, in general, involves no symmetry change between two phases. Since we do not expect translational invariance for disordered Wigner crystal, the metal and the insulator do not differ by any static symmetry. Thus, strictly speaking, it does not display a quantum critical point. However, since $T = T_c$ is an extremely small temperature scale, of the order of only a few percent of the Fermi temperature, the behavior at $T \gg T_c$ features a very well developed quantum critical (QC) region displaying universal scaling behavior of the resistivity curves. This QC region is centered around the so-called quantum Widom line (QWL), which shows characteristic back-bending at higher temperatures. Experimentally, the QWL is identified by locating the inflection point of the resistivity curves obtained by tuning through a transition at fixed temperature. This quantum critical scaling behavior, which was theoretically predicted in a seminal 2011 paper [16], was soon confirmed in spectacular detail in a series of experiments on Mott or-

ganics by Kanoda and collaborators [15,19], including the characteristic "mirror symmetry" of the scaling function, as also predicted by theory.

Further out on the metallic side, the family of curves were predicted to display resistivity maxima at $T = T_c \times \delta$, marking the onset of quasiparticle transport and the formation of the strongly correlated electron liquid at lower temperatures. Here, the parameter δ measures the distance from the MIT, which can be accessed by tuning the bandwidth (pressure) or the carrier density in the system. These theoretical predictions provided a clear and precise guidance for experiments, defining a procedure that should be utilized to detect the effects of strong correlations in the vicinity of the Mott transition [14]. The experimental work has largely confirmed essentially all the expected features of the MIT critical region, in those systems where the MIT undeniably has Mott character [20]. The remaining challenge, therefore, is to seek further validation of this scenario in other systems where Mottness is less obvious as the controlling mechanism, which is what we achieve in the present study.

II. RESULTS AND DISCUSSIONS

We now explore the possible presence of Mott quantum criticality in few-layered molybdenum disulfide (MoS_2) following a proposed procedure based on theory. In general, 2D materials require the substrate, which strongly restricts the mobility. On the other hand, the ineffective screening enhances interactions between electrons. Furthermore, the large effective electron mass, $m^* \sim 0.5 m_e$, and the small dielectric constant $\varepsilon \sim 8$ for multilayer [21], giving the large dimensionless interaction parameter $r_s \equiv E_C/E_F \propto m^*/\varepsilon\sqrt{n_{2D}} \sim 9$ at $n_{2D} \sim 3 \times 10^{12}$ cm^{-2}, are the favorable factors for the observation of Mott-like transition in MoS_2. Here, m_e is the free electron mass, E_C is the Coulomb energy, E_F is the kinetic (Fermi) energy, and n_{2D} is the carrier density. In this n-type 2D semiconducting material, the Mott-like transition is pictured as the one from the strongly correlated metallic electron liquid state to the charge ordered insulating state (Wigner crystallization) as the carrier density decreases in the conduction band, as shown in Fig. 1(a).

In the following we present our experimental data obtained for this material. The inset in Fig. 1(b) shows the optical image of $\sim$7-nm-thick MoS_2 (5.5 μm in length and 4.5 μm in width) with four-probes on the SiO_2 (300 nm)/Si (heavily p-doped) substrate. Figure 1(b) displays the resistivity ρ in the unit of quantum resistance h/e^2 for the chosen backgate biases, extracted in the zero drain-source voltage limits (see Appendix A). Observing two sharply distinct families of curves $\rho(T)$, $\Delta\rho/\Delta T > 0$ and $\Delta\rho/\Delta T < 0$, suggests the metal-insulator transition at a critical backgate bias $V_c \sim 21$ V at low temperature. We also note the pronouncedly nonmonotonic temperature dependence of resistivity in the metallic phase. The peak value near the transition exceeds the upper bound $\rho_c \leqslant (2/n_s n_v)h/e^2$ predicted by the Mott-Ioffe-Regel theory [22], where n_s is the spin and n_v is the valley degeneracy: $n_s = 2$ and $n_v = 6$ for multilayer MoS_2 [23]. Also, the resistivity maximum occurs at the temperature $T^* \sim 20$ K much lower than the Fermi temperature $T_F \sim 200$ K. Very similar behavior of the resistivity has been reported in organic
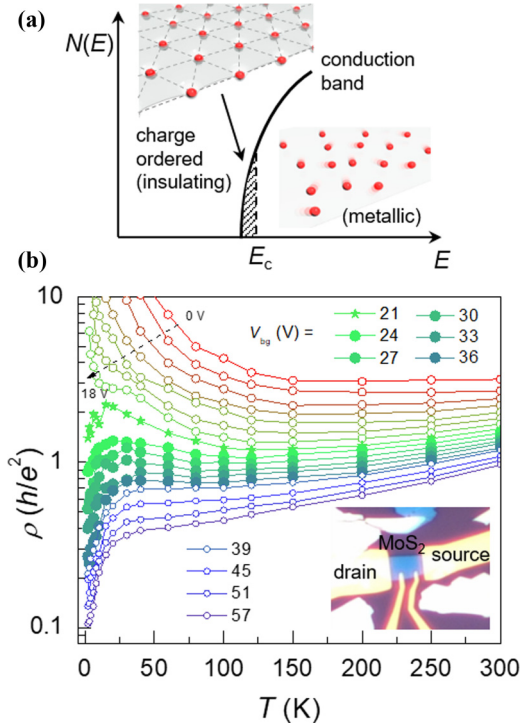
FIG. 1. (a) Schematic view of metal-insulator transition. (b) Electric resistivity (ρ) as a function of temperature (T) for various backgate biases V_{bg}. Inset shows the optical image of multilayer MoS$_2$ device.

Mott systems [24] and only in particularly clean 2D systems [1,25], and it has been interpreted to originate from strong correlation effects. In some sense, the observation of such features in multilayer MoS$_2$ of rather low field effect mobility $\mu \approx 1500\,\text{cm}^2\,\text{V}^{-1}\,\text{s}^{-1}$ at 2 K (see Appendix B) might, at a first glance, look surprising. In addition, the Fermi energy in this system is $T_F \sim 200$ K, much higher compared to standard high mobility 2DEGs where it is typically around 10 K. From the theoretical perspective, however, only relative

energy scales are significant, and those are comparable in both systems. As we mentioned earlier, MoS$_2$ has a strong correlation due to the large effective mass and poor screening.

In order to check the possibility of Mott quantum criticality in this material, we next perform the scaling analysis of the resistivity maxima based on the theoretical predictions for the Hubbard model. Assuming the resistivity of the form, $\rho(T) = \rho_0 + \delta\rho(T)$ where ρ_0 is the residual resistivity due to impurity scattering and $\delta\rho(T)$ is the temperature dependent resistivity dominated by electron-electron scattering, the scaling form was proposed as [14]

$$\delta\rho(T) = \delta\rho_{max} f(T/T_{max}), \qquad (1)$$

where $\delta\rho_{max} = \rho_{max} - \rho_0$ and ρ_{max} is the maximum resistivity at $T = T_{max}$.

Following this scheme, we now perform the scaling of resistivity for five different backgate biases V_{bg}, as shown in Fig. 2(a), and they display an excellent collapse. When we compare the collapsed data to the scaling curve theoretically predicted for a single band Hubbard model at half filling (blue curve, which also coincides with the collapsed curve of 2DEGs in silicon) [14], we do notice a certain systematic discrepancy. In the following, we argue that this discrepancy is due to disorder that is significantly higher than in 2DEGs. For this purpose, we extended previous theoretical calculation to include moderate disorder, and investigate how this affects the scaling of the resistivity maxima. We consider a disordered Hubbard model at half filling, where disorder is modeled as a site diagonal random potential chosen from uniform distribution in the energy range $[-W/2,\ W/2]$. We treat disorder on the level of coherent potential approximation (CPA) [26], treating the correlation effects using DMFT theory, the same technique as in previous work (see Appendix C). A moderate strength of disorder of $W = 2.5$, in the unit of half-bandwidth, allows us to match disordered DMFT scaling function with our collapsed data. Now we clearly see the effects of disorder, i.e., it simply produces a slight broadening of the scaling function, reflecting the effect of disorder to broaden the bandwidth of the electronic spectrum [27] (see Appendix D for a similar
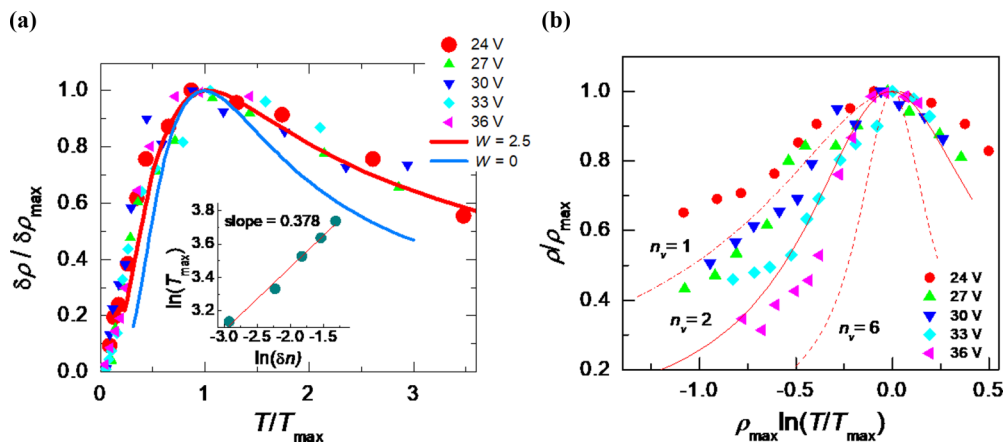

FIG. 2. (a) Normalized resistivity as a function of normalized temperature for five consecutive V_{bg}. The blue and the red solid lines are the theoretical scaling results from the Hubbard model with a disorder strength $W = 0$ and 2.5, respectively. Inset shows T_{max} as a function of a reduced carrier density δn. (b) Normalized resistivity as a function of $\rho_{max}\ln(T/T_{max})$. Dash-dot, solid, and dash lines are the theoretical scaling curves corresponding to the valley degeneracy $n_v = 1$, 2 and 6, respectively.
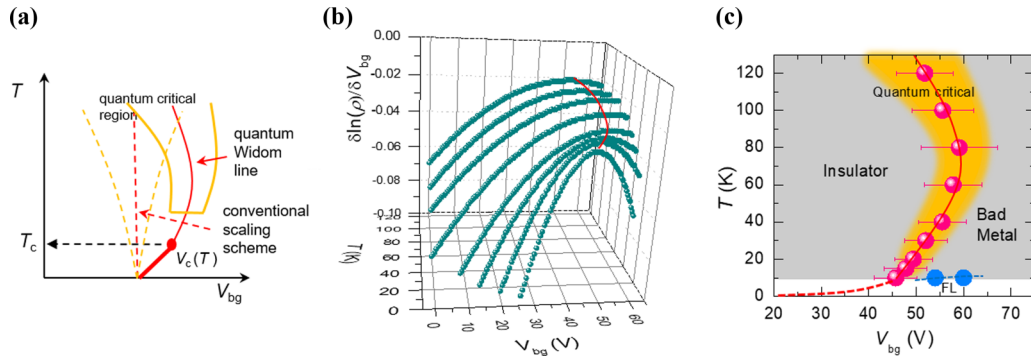
FIG. 3. (a) Schematic phase diagrams and quantum critical regions (confined by yellow lines) for the conventional MIT picture (temperature independent V_c, dashed red line) and the Mott MIT (temperature dependent V_c, solid red line). (b) The derivatives of fitting functions to $\ln(\rho)$ with respect to V_{bg} for temperatures from 10 to 120 K. The red line is the QWL connecting maxima. (c) Phase diagram of multilayer MoS$_2$. The red dashed line is the simple interpolation to $V_c \sim 21$ V at the lowest temperature.

result with a thinner sample). These disorder effects, however, are only quantitative changes that should not introduce any significant qualitative modifications to the quantum critical behavior at the Mott point [27]. The use of CPA approximation here is completely justified, since the considered disorder level is moderate and we should be far from the Anderson (disorder-driven) metal-insulator transition. In addition, the observed power law dependence of T_{max} as a function of the reduced carrier density $\delta n = (n - n_c)/n_c$ as shown in the inset of Fig. 2(a) supports this expectation. Here, n_c is the critical carrier density. This remarkable scaling description strongly suggests the Mott-like transition in multilayer MoS$_2$.

From a different point of view, Finkel'stein and Punnoose [28,29] developed a theory that describes the nonmonotonic temperature dependence of resistivity as a result of the competition between disorder and interactions. In this theory, the metallic state is stabilized by the strong correlation and the localization is driven by disorder. However, we find that the scaling based on this theory is poor as shown in Fig. 2(b), in which experimental data do not collapse to any one of the theoretical scaling curves corresponding to the number of valley degeneracy n_V (see Appendix E for more discussion), making us more confident to pursue more analysis for Mott criticality in this multilayer MoS$_2$.

Previous scaling analyses of the experimental results on 2DMITs have been made along the temperature-independent critical transition-driving parameter, i.e., n or V_{bg} in our case, as schematically shown in Fig. 3(a) (red dashed line). The Mott transition is, however, a first-order phase transition at low temperature, and the critical scaling behavior is expected above the critical end point T_c. In this case, for the quantum critical scaling, it is essential to identify the instability trajectory where the system is least stable, called the quantum Widom line (QWL) [16,30,31], which separates metal and insulator, and is usually temperature dependent as shown in Fig. 3(a) (red solid line). There are several ways to define the QWL but it is known that the scaling behavior is not so sensitive to the choice of them [31]. We find the QWL from the inflection points in $\ln \rho(V_{bg}, T)$ vs V_{bg} curves. To identify the inflection points, $(V_c(T), \rho_c(T))$, we first fit the data $\ln \rho(V_{bg}, T)$ by a polynomial for each temperature, and

differentiate it with respect to V_{bg} to find the maximum. Figure 3(b) exhibits the resulting figure for T and V_{bg}, and the red line that connects the maximal points is the QWL. Figure 3(c) shows the consequential phase diagram. The error bars are determined from the raw data (see Appendix F for more details). The dashed line is the interpolation to the $V_c \sim 21$ V at the lowest temperature. The QWL exhibits the same nonmonotonic form as in organic systems [15]. In these organic systems in which the phase transition is driven by the pressure, the positive slope of the QWL reflects the large entropy of localized spins on the insulating side, consistent with Clausius-Clapeyron equation. The close similarity in Fig. 3(c) strongly suggests the formation of local moment, i.e., Mott localization in this multilayer MoS$_2$. The slope change at high temperature is due to the thermal filling of the Mott gap. Two blue points define the boundary between the bad metal and the Fermi liquid obtained from the inflection points in $\rho(V_{bg}, T)$ vs T (see Appendix F) [31].

Based on the QWL in Fig. 3(c), we plot the normalized resistivity ρ/ρ_c as a function of δV_{bg} for several temperatures in Fig. 4(a), where $\delta V_{bg} = V_{bg} - V_c(T)$. All traces cross at $\delta V_{bg} = 0$, the transition point between metal and insulator. Then, we rescale δV_{bg} for each trace at different temperature by $w(T)$ so that all curves collapse into a universal one in ρ/ρ_c vs $\delta V_{bg} w(T)$ as shown in Fig. 4(b). Figure 4(c) displays the scaling parameter w for temperature in log scale. The dynamical mean-field theory (DMFT) predicts that the resistivity scaling holds above $\sim 2 T_c$. In fact, the linear, i.e., power law behavior in the inset appears in the temperature range $20 \lesssim T \lesssim 80$ K. We extract the exponent $z\nu$ from the slope via $w(T) \sim T^{-1/z\nu}$, where ν is the critical exponent of the correlation length and z is the dynamical critical exponent. From the linear fit, we obtain $z\nu = 2.56 \pm 0.37$.

As usually expected for quantum criticality, the resistivity should follow the scaling relation $\rho(T, \delta V) = \rho_c(T) f[T/T_0(\delta V)]$, where $T_0 = |c\delta V|^{z\nu}$ with an arbitrary constant c. With a value $z\nu = 2.56$ along the QWL, all curves of ρ/ρ_c in the scaling regime of temperature collapse into two branches of insulator and metal, respectively, as shown in Fig. 5. The scaling along the temperature-independent $V_c = 21$ V causes nonequal $z\nu$ values for the insulating and the
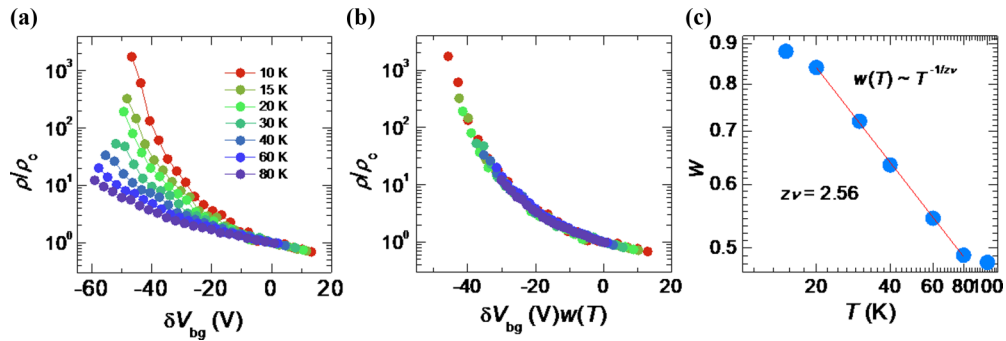
FIG. 4. (a) The normalized resistivity for the adjusted backgate bias $\delta V_{bg} = V_{bg} - V_c(T)$ by the critical backgate bias $V_c(T)$ along the QWL. (b) Scaling plot of normalized resistivity for rescaled δV_{bg} by scaling parameter $w(T)$. (c) Scaling parameter as a function of temperature in log-log scale.

metallic sides (see Appendix G). We believe that this is the result from the incorrect scaling for the Mott criticality in this system. The scaling for all reported 2DMIT phenomena have been performed in the latter scheme. The asymmetric zv across the 2DMITs in a certain system might be amended in a Mott scaling picture [32].

The critical exponent $zv = 2.56$ for multilayer MoS$_2$ is rather large, different than in other systems in which the Mott transition is speculated. The DMFT calculation estimates [16] $zv = 0.56$–0.57, and the experiments in organic materials report the similar values [15], $zv = 0.49$–0.68. Although the organic materials and our multilayer MoS$_2$ share several similar Mott features, the distinctly different zv suggests that they belong to very different universality classes. In fact, the DMFT predicts $zv = 1.35$ for the doped case [30], in which the transition is driven by electrically doping the system, as usually has been implemented in 2D systems such as Si MOSFETs. This theory is based on the single band Hubbard model without intersite interactions. The values of zv in clean Si MOSFETs [1,2] are 1.2–1.6, comparable to the above theo-

retical value, but we note that these experimental results were not based on the Mott picture using the Widom line.

III. CONCLUSIONS

Including intersite interactions, the Wigner crystallization similar to Mott physics can occur for any partially filled band in the low carrier-density limit, requiring charge ordering with local magnetic moments [13]. The precise role of such charge ordering in the vicinity of the transition has not been investigated from the theoretical perspective although most reported experimental results in 2D systems correspond to this type of transition. Besides, the difference in the underlying band structure or the form of the lattice is known to likely originate various Mott systems with different critical exponents.

The Mott transition in 2D systems has not been clearly demonstrated. Even in the cleanest Si MOSFETs, the non-monotonic temperature dependent resistivity in the metallic phase near the MIT has often been interpreted as a result of a dominating correlation effect in disorder-driven localization. In this disorder scenario, the scaling behavior by the normalization group equation generally applies to only few traces near the MIT [8,29]. We showed that the nonmonotonic behavior in multilayer MoS$_2$ is excellently explained by the scaling in the Mott picture with disorder for the wide range of carrier density but poorly in a disorder scenario. Moreover, the successful scaling with one zv value for both metallic and insulating phases using the temperature dependent Widom line strongly suggests the Mott-like transition in a 2D system.
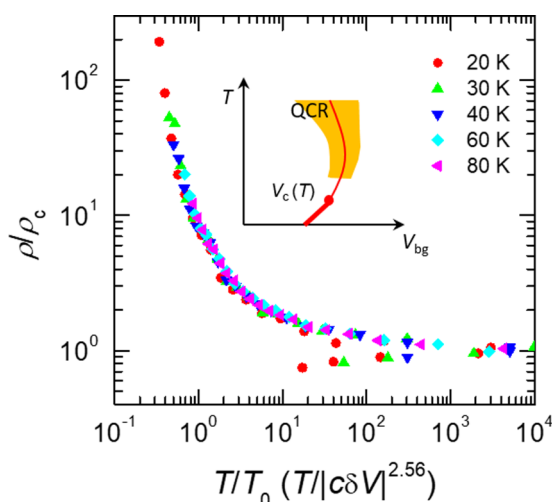
FIG. 5. Scaling of normalized resistivity for normalized temperature by $T_0 = |c\delta V|^{zv}$ with the given value of $zv = 2.56$. Inset shows the schematic phase diagram based on the Widom line.
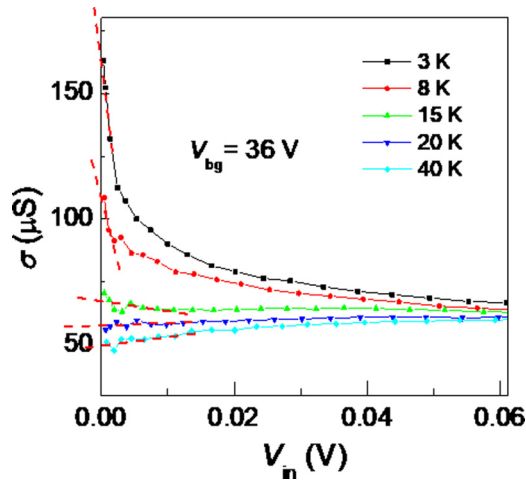
FIG. 6. Extraction of conductivities in the zero voltage limit.

Scientific Computing Laboratory of the Institute of Physics Belgrade.

APPENDIX A: EXTRACTION OF CONDUCTIVITIES

In order to obtain the conductivity in the zero voltage limit, we measure the conductivity as a function of a drain-source voltage or voltage between two inner probes V_{in}, and simply extrapolate the conductivity to the zero voltage limit. Figure 6 shows the example of extracting the conductivity by linearly extending the low field data (red dashed lines) to the zero voltage limit at $V_{bg} = 36\,\text{V}$ for various temperatures.

APPENDIX B: FIELD EFFECT MOBILITY

The mobility in Fig. 7 is obtained from the conductivity extracted in the zero voltage limit.
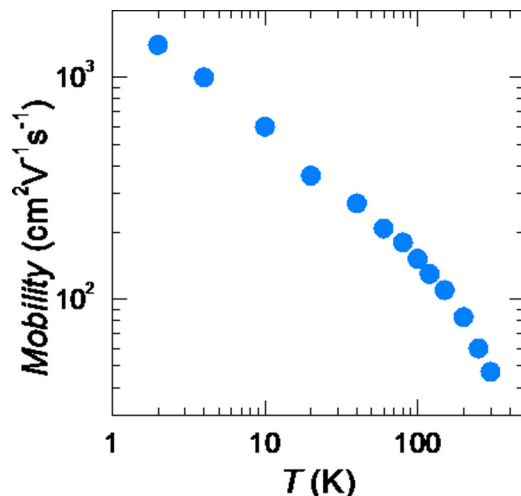

FIG. 7. Field effect mobilities as a function of the temperature.

APPENDIX C: RESISTIVITY SCALING CURVE OF DISORDERED HUBBARD MODEL

For the purpose of investigation of disorder effects in strongly correlated systems we consider the half-filled single-orbital Hubbard model with site-diagonal disorder and nearest neighbor hopping,

$$H = -\sum_{i,j,\sigma} t_{i,j} c_{i\sigma}^{\dagger} c_{j\sigma} + U \sum_i n_{i\uparrow} n_{i\downarrow} + \sum_{i\sigma} v_i n_{i\sigma} - \mu \sum_{i\sigma} n_{i\sigma},$$

$$(C1)$$

where $t_{i,j}$ is the nearest neighbor hopping amplitude, $c_{i\sigma}^{\dagger} (c_{i\sigma})$ are charge carrier creation (annihilation) operators, and $n_{i\sigma} = c_{i\sigma}^{\dagger} c_{i\sigma}$ is the occupation number operator on site i for spin σ. Interaction is described by the interaction strength parameter U, μ is the chemical potential chosen to impose half filling, and v_i is the random on-site potential (source of disorder). We choose v_i from uniform distribution, since most of the features of the disordered Hubbard model (DHM) are expected to be insensitive to the particular form of the disorder distribution.

In the spirit of DMFT, DHM can be reduced to the ensemble of Anderson impurity models in a self-consistently determined conduction bath. Here we consider an ensemble of impurities, and we use the coherent potential approximation (CPA) to close the set of self-consistent equations of the disordered Hubbard model. Within the CPA we solve an impurity model for each on-site energy, and we average Green's functions,

$$G_{av}(i\omega) = \frac{1}{N} \sum_{i=1}^{N} G_i(i\omega).$$

$$(C2)$$

From the averaged Green's function we calculate dynamical mean field and from this point DFMT equations are analogous to those in the clean case.

The optical conductivity σ is calculated using the Kubo formula, and dc resistivity is defined as

$$\rho_{dc} = [\text{Re}\,\sigma(\omega = 0)]^{-1}.$$

$$(C3)$$

Further, we apply a scaling ansatz (we divide the resistivity by the maximum of the resistivity ρ/ρ_{max} and the temperature by the temperature where the maximum is reached, T/T_{max}) to all metallic curves close to the transition, and we collapse all resistivity curves to the single scaling curve of DHM. The scaling curve is well defined outside of the Fermi-liquid region.

APPENDIX D: SCALING RESULT FOR A THINNER SAMPLE BASED ON HUBBARD MODEL

Figure 8 shows a temperature dependent resistivity for several backgate biases (a) and the phenomenological scaling result based on the Hubbard model for a thinner sample of 3.5 nm in thickness. As shown in Fig. 8(a), the MIT occurs at $V_{bg} \sim 43\,\text{V}$, and the important feature of nonmonotonic temperature-dependent resistivity near MIT in the metallic phase is clearly reproduced. Figure 8(b) shows that the tendency of a scaling result agrees well with a theoretical prediction.
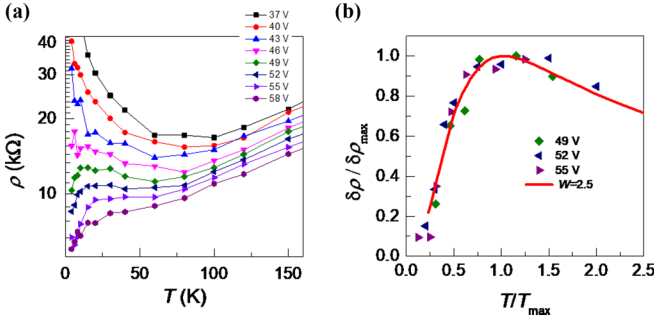
(a) **(b)**

FIG. 8. (a) ρ vs T for several V_{bg}. (b) Normalized resistivity as a function of normalized temperature for three consecutive V_{bg}. The red solid line is the theoretical scaling result from the Hubbard model with a disorder strength $W = 2.5$.

FIG. 9. Normalized resistsivity as a function of $\rho_{max}\ln(T/T_{max})$. Dash-dot, solid, and dash lines correspond to the valley degeneracy $n_v = 1$, 2, and 6, respectively. The inset shows the behavior of γ_2^* as a function of n_v.

APPENDIX E: SCALING ANALYSIS USING FINKELSTEIN AND PUNNOOSE'S THEORY

The nonmonotonic temperature dependent resistivity in the metallic phase near the MIT has been observed only in very clean systems such as 2D electrons in Si MOSFET [33] and 2D holes in GaAs [34]. In this sense, it is surprising that multilayer MoS$_2$ of $\mu \approx 1500$ cm^2 V^{-1} s^{-1} shows a similar feature. Finkel'stein and Punnoose [7,28,29] described this behavior as a result of a competition between the weak localization ("Cooperon" contribution, particle-particle channel) and spin-valley multiplet modes of interactions for antilocalization ("Diffuson" contribution, particle-hole channel). They derived following coupled renormalization group (RG) equations to describe the flow of the resistivity ρ and the interaction amplitude γ_2 for valley degeneracy n_v:

$$\frac{dr}{d\zeta} = r^2\left[n_v + 1 - \left(4n_v^2 - 1\right)\left(\frac{1+\gamma_2}{\gamma_2}\ln(1+\gamma_2) - 1\right)\right],$$
(E1)

$$\frac{d\gamma_2}{d\zeta} = r\frac{(1+\gamma_2)^2}{2},$$
(E2)

where $r = (e^2/\pi h)\rho$, $\zeta = -\ln(T\tau)$, and τ is the elastic scattering time. Dividing Eq. (E1) by (E2) gives

$$\frac{dr}{d\gamma_2} = \frac{2r\left[n_v + 1 - \left(4n_v^2 - 1\right)\left(\frac{1+\gamma_2}{\gamma_2}\ln(1+\gamma_2) - 1\right)\right]}{(1+\gamma_2)^2}.$$
(E3)

The dimensionless parameter r for the resistivity has a maximum r_{max} at γ_2^* satisfying $dr/d\gamma_2 = 0$. γ_2^* decreases as n_v increases as shown in the inset of Fig 8. In particular, a considerable decrease occurs when n_v changes from 1 to 2. Since γ_2 increases monotonically as T decreases and r starts decreasing when γ_2 becomes larger than γ_2^*, the decrease of γ_2^* indicates that antilocalization can occur more easily. From this aspect, multivalley systems are more advantageous to observe MIT phenomena. Following Ref. [29], the universal function $R(\eta)$ is defined via $r = r_{max}R(\eta)$ and $\eta = r_{max}\ln(T_{max}/T)$, where T_{max} is the temperature at which $r(T_{max}) = r_{max}$ and $\gamma_2(T_{max}) = \gamma_2^*$. By integrating Eqs. (E2) and (E3) numerically with the boundary conditions $r(\zeta = 0) = r_{max} = 1$ and
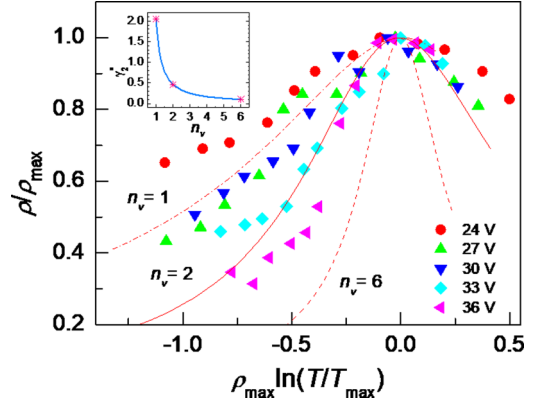
$\gamma_2(\zeta = 0) = \gamma_2^*$, $R(\eta)$ can be obtained without any fitting parameter. In Fig. 9, we plot this function corresponding to $n_v = 1$ (dash-dot line), 2 (solid line), and 6 (dash line) with normalized data for $V_{bg} = 24$–36 V. As seen in this figure, the collapse of data is very poor, so that the theory by Finkel'stein
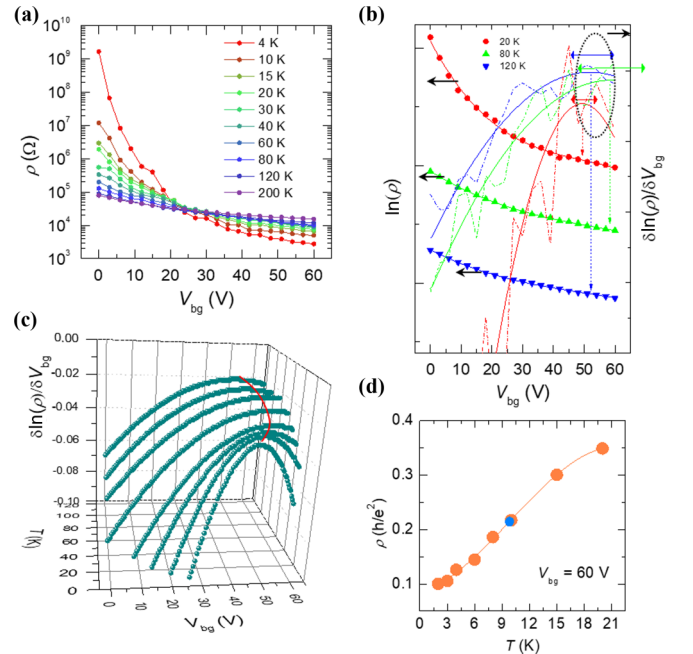

(a) **(b)** **(c)** **(d)**

FIG. 10. (a) ρ vs $V_{bg}(V)$. (b) Determination of the critical back-gate biases $V_c(T)$ from inflection points in $\ln(\rho)$ vs $V_{bg}(V)$. Inflection points are the extrema in $\delta\ln(\rho)/\delta V_{bg}$ vs $V_{bg}(V)$. Solid lines are fits of $\ln(\rho)$ by polynomials (left axis) and their derivatives with respect to V_{bg} (right axis). Dashed lines are derivatives of the raw data. Traces are shifted for the clarity. Colored arrows indicate the error ranges for the traces of the same colors in the determination of inflection points from raw data. (c) The derivatives of fitting functions to $\ln(\rho)$ with respect to V_{bg} for temperatures from 10 to 120 K. The extrema are inflection points in $\ln(\rho)$ vs $V_{bg}(V)$. (d) The inflection point in ρ vs T defines the boundary between the bad metal and the Fermi liquid.
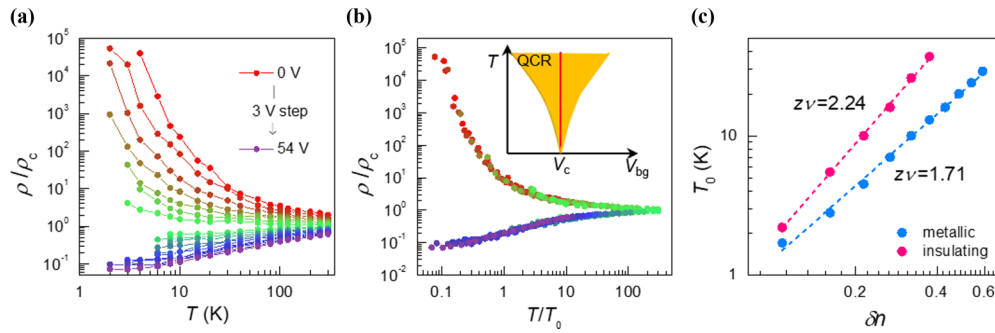
FIG. 11. (a) Normalized resistivity ρ/ρ_c as a function of temperature for V_{bg} from 0 to 54 V in a 3-V step. (b) ρ/ρ_c as a function of normalized temperature T/T_0. Inset shows the temperature-independent critical backgate bias and the quantum critical region around it. (c) Scaling parameters T_0 as a function of the reduced carrier density δn.

and Punnoose seems improper to describe the nonmonotonic conductivity behavior in the metallic phase near the MIT.

APPENDIX F: DETERMINATION OF THE QUANTUM WIDOM LINE

As we stated in the main text, the quantum Widom line (QWL) can be determined in several different ways. Although each method gives a different QWL to some extent, the scaling behavior is known to be insensitive to its choice. One of the easiest ways from the experimental point of views is to find the inflection points in $\ln \rho(V_{bg}, T)$ vs V_{bg} curves. Figure 10(a) shows the resistivity as a function of the backgate bias. In Fig. 10(b), we show the fittings to the data points of $\ln \rho(V_{bg}, T)$ using polynomials for chosen temperatures in the left axis, and their first derivatives with respect to the backgate bias in the right axis. Dashed lines are derivatives of the raw data. All traces are shifted for the clarity. Figure 10(c) exhibits the complete set of these first derivatives for the temperature range we choose for the scaling. The red line connecting the extrema of the curves is the QWL, giving the result shown in Fig. 4(b) in the main text. From the inflection point in Fig. 10(d), the boundary between the bad metal and the Fermi liquid at $V_{bg} = 60$ V is determined.

APPENDIX G: CONVENTIONAL SCALING ANALYSIS

For the metal-insulator transition when it is considered as a second order phase transition, the scaling behavior can be represented as $\rho(T, \delta n) = \rho_c(T)F[T/T_0(\delta n)]$, where F is a universal scaling function, ρ_c is the temperature-

dependent critical resistivity at the critical backgate bias V_c, and $T_0(\delta n) \sim |\delta n|^{z\nu}$. Here, the reduced carrier density δn is defined as $\delta n = \frac{n - n_c}{n_c}$ with a critical carrier density n_c (or critical backgate voltage V_c) which is independent of the temperature. Following this law, we perform the scaling analysis as shown in Fig. 11 below. Figure 11(a) displays the normalized conductivity ρ/ρ_c as a function of the temperature for various backgate biases. The normalization of the temperature by the scaling parameter T_0 is, then, performed until each trace collapses into one for the metallic and the other for the insulating phases, as shown in Fig. 11(b). From the power law behavior of T_0 for δn, the critical exponent $z\nu$ is determined, as shown in Fig. 11(c). This scaling scheme corresponds to the scaling along the temperature-independent $V_c = 21$ V, as shown in the inset of Fig. 11(b). We think that the asymmetric $z\nu$ for the metallic and insulating phases results from the incorrect scaling for the Mott criticality in this system, as we described in the main text.

APPENDIX H: METHODS

Multilayer MoS_2 was mechanically exfoliated on a highly doped 300 nm SiO_2/Si substrate. To pattern the electrodes, PMMA A4 was spin-coated (3000 rpm, 50 s) and then, the electron beam lithography (EBL) was performed, followed by Cr/Au (1/60 nm) evaporation in high vacuum ($\sim 10^{-6}$ Torr). Four-probe electrical measurements were performed in high vacuum ($\sim 10^{-6}$ Torr) using a cryostat (PPMS, Quantum Design, Inc.) with a characterization system (B1500A, Keysight Technologies).

[1] S. V. Kravchenko, W. E. Mason, G. E. Bowker, J. E. Furneaux, V. M. Pudalov, and M. Dlorio, Phys. Rev. B **51**, 7038 (1995).

[2] S. V. Kravchenko, D. Simonian, M. P. Sarachik, W. Mason, and J. E. Furneaux, Phys. Rev. Lett. **77**, 4938 (1996).

[3] D. Popovic, A. B. Fowler, and S. Washburn, Phys. Rev. Lett. **79**, 1543 (1997).

[4] D. Simonian, S. V. Kravchenko, and M. P. Sarachik, Phys. Rev. B **55**, R13421 (1997).

[5] V. Dobrosavljevič and D. Tanasković, in *Strongly Correlated Electrons in Two Dimensions*, edited by S. Kravchenko (Pan Stanford Publishing, Singapore, 2017), p.1–46.

[6] S. Kravchenko and M. Sarachik, Rep. Prog. Phys. **67**, 1 (2003).

[7] A. Punnoose and A. M. Finkel'stein, Science **310**, 289 (2005).

[8] S. Anissimova, S. Kravchenko, A. Punnoose, A. Finkel'Stein, and T. Klapwijk, Nat. Phys. **3**, 707 (2007).

[9] J. S. Thakur and D. Neilson, Phys. Rev. B **59**, R5280 (1999).

[10] B. Spivak, Phys. Rev. B **64**, 085317 (2001).

[11] S. Pankov and V. Dobrosavljević, Phys. Rev. B **77**, 085104 (2008).

[12] A. Camjayi, K. Haule, V. Dobrosavljević, and G. Kotliar, Nat. Phys. **4**, 932 (2008).

[13] A. Amaricci, A. Camjayi, K. Haule, G. Kotliar, D. Tanasković, and V. Dobrosavljević, Phys. Rev. B **82**, 155102 (2010).

[14] M. M. Radonjić, D. Tanasković, V. Dobrosavljević, K. Haule, and G. Kotliar, Phys. Rev. B **85**, 085133 (2012).

[15] T. Furukawa, K. Miyagawa, H. Taniguchi, R. Kato, and K. Kanoda, Nat. Phys. **11**, 221 (2015).

[16] H. Terletska, J. Vucicevic, D. Tanaskovic, and V. Dobrosavljevic, Phys. Rev. Lett. **107**, 026401 (2011).

[17] G. H. Han, D. L. Duong, D. H. Keum, S. J. Yun, and Y. H. Lee, Chem. Rev. **118**, 6297 (2018).

[18] S. Manzeli, D. Ovchinnikov, D. Pasquier, O. V. Yazyev, and A. Kis, Nat. Rev. Mater. **2**, 17033 (2017).

[19] M. Urai, T. Furukawa, Y. Seki, K. Miyagawa, T. Sasaki, H. Taniguchi, and K. Kanoda, Phys. Rev. B **99**, 245139 (2019).

[20] Y. Kurosaki, Y. Shimizu, K. Miyagawa, K. Kanoda, and G. Saito, Phys. Rev. Lett. **95**, 177001 (2005).

[21] X. Chen, Z. Wu, S. Xu, L. Wang, R. Huang, Y. Han, W. Ye, W. Xiong, T. Han, G. Long, Y. Wang, Y. He, Y. Cai, P. Sheng, and N. Wang, Nat. Commun. **6**, 6088 (2015).

[22] S. Das Sarma and E. H. Hwang, Phys. Rev. B **89**, 121413(R) (2014).

[23] J. Hong, C. Lee, J.-S. Park, and J. H. Shim, Phys. Rev. B **93**, 035445 (2016).

[24] P. Limelette, P. Wzietek, S. Florens, A. Georges, T. A. Costi, C. Pasquier, D. Jérome, C. Mézière, and P. Batail, Phys. Rev. Lett. **91**, 016401 (2003).

[25] Y. Hanein, U. Meirav, D. Shahar, C. C. Li, D. C. Tsui, and H. Shtrikman, Phys. Rev. Lett. **80**, 1288 (1998).

[26] V. Dobrosavljević and G. Kotliar, Phys. Rev. B **50**, 1430 (1994).

[27] M. M. Radonjić, D. Tanasković, V. Dobrosavljević, and K. Haule, Phys. Rev. B **81**, 075118 (2010).

[28] A. M. Finkel'stein, Sov. Phys. JETP **57**, 97 (1983).

[29] A. Punnoose and A. M. Finkel'stein, Phys. Rev. Lett. **88**, 016802 (2001).

[30] J. Vučičević, D. Tanasković, M. J. Rozenberg, and V. Dobrosavljević, Phys. Rev. Lett. **114**, 246402 (2015).

[31] J. Vučičević, H. Terletska, D. Tanasković, and V. Dobrosavljević, Phys. Rev. B **88**, 075143 (2013).

[32] B. H. Moon, J. J. Bae, M.-K. Joo, H. Choi, G. H. Han, H. Lim, and Y. H. Lee, Nat. Commun. **9**, 2052 (2018).

[33] S. V. Kravchenko, G. V. Kravchenko, J. E. Furneaux, V. M. Pudalov, and M. D'Iorio, Phys. Rev. B **50**, 8039 (1994).

[34] J. Yoon, C. C. Li, D. Shahar, D. C. Tsui, and M. Shayegan, Phys. Rev. Lett. **82**, 1744 (1999).